

A REEVALUATION OF THE LIFT FORCE IN EULERIAN MULTIPHASE CFD

R. Sugrue and E. Baglietto

Department of Nuclear Science and Engineering, Massachusetts Institute of Technology
77 Massachusetts Avenue, Cambridge, MA 02139, USA
rsugrue@mit.edu

ABSTRACT

This paper describes the progress achieved towards the development of a new approach for modeling hydrodynamic closures in multiphase computational fluid dynamics (M-CFD), and specifically focuses on the analysis of the lift force implementation, which has proved to be a critical challenge. While existing formulations of the lift force (e.g. Tomiyama et al.) have been extensively applied with mixed success, no rigorous verification and validation on fundamental unit tests had been performed previous to this work. Baseline test cases on the drag force are presented, along with the extensive work on the formulation, implementation, and testing of the lift force. Promising results are shown that have the potential to benefit the advancement of M-CFD towards robust industrial applications.

KEYWORDS

Lift force, multiphase CFD, hydrodynamic closure, two-phase flow

1. INTRODUCTION & OBJECTIVES

Multiphase flow analysis of reactor cores has long been dependent upon sub-channel analysis codes, which are a practical approach to implement experimentally derived correlations into an accurate core wide analysis tool. The lumped channel averaged approach clearly eliminates the capability of accounting for detailed 3-dimensional intra-channel effects. Furthermore and most importantly, the adopted set of correlations makes them applicable only to a specific range of geometrical and physical conditions, which should not be further extrapolated. Based on the general validity of the underlying Navier-Stokes approach and the 3-dimensional local resolution of two-phase flow, multiphase computational fluid dynamics (M-CFD) modeling has the potential to overcome the weaknesses of current industry approaches. The most promising M-CFD framework is represented by the Eulerian-Eulerian, two-fluid model with or without an interfacial area transport. This time and space averaged approach requires closure relations for the phase-to-phase and wall-to-flow mass, momentum, and energy terms in the governing equations. The current challenge is therefore the development of generally applicable closure methods [1].

Closure relations for viscous drag, lateral lift, virtual mass, turbulence dispersion, and wall lubrication have been developed in the past, but not specifically for CFD, which requires the adoption of a more local modeling approach, independent of any global information. Thus, the motivation of this work has been to develop a new momentum closure approach in CFD, for PWR applications, which should demonstrate improved robustness in order to be applicable to a vast range of geometries, void fractions, and flow regimes. The current efforts have mainly been focused on the formulation, implementation, and testing of the lift force, which has shown to be the most critical challenge in M-CFD applications. While existing formulations (e.g. Tomiyama et al.) have been extensively applied with mixed success, no rigorous verification on fundamental unit tests had been performed previous to this work, and the complex interaction of closure forces does not allow for full judgment of the influence of lift in integral tests.

A plethora of experimental, analytical, and numerical studies have investigated various fluids and channel geometries, as well as flow regimes and other conditions to develop and validate models for lift and drag closure relations. The experimental work has involved collecting data for development of closure relations by several methods, including high speed video camera (HSV), charged-coupled device (CCD) camera coupled with a microscope, particle image velocimetry (PIV), laser Doppler anemometry (LDA), and wire-mesh sensors. These studies typically measure bubble size, velocity, and separation distance from the wall in order to evaluate various components of the hydrodynamic force.

One example of an experimental study suitable for CFD applications is Takemura et al. [2, 3, 4] who worked with a CCD camera and microscope in order to measure bubble radius, contour and rise velocity, and the distance between the bubble and the wall to calculate drag and lift components of the hydrodynamic force. Tomiyama et al. [5] used a HSV camera to measure trajectories and shapes of single air bubbles in simple shear flows of glycerol-water solution to evaluate the transverse lift force acting on single bubbles.

Among the numerical simulations is the work of Legendre and Magnaudet [6] who calculated the shear lift force on a sphere over a large range of Reynolds numbers and several values for shear rates (Sr). Rastello et al. [7, 8] also have recently conducted experiments which produce results that match reasonably well with Legendre and Magnaudet's data.

From an analytical perspective, studies have investigated both the flow of a simple shear around a sphere for low particle Reynolds number [9] and the inviscid limit of weak simple shear around a sphere [10, 11]. Saffman initially investigated low Reynolds number flow and developed an expression for the lift force which became the basis for subsequent studies. His work, however, did not consider wall effects [9], which was corrected subsequently by McLaughlin [12] and by Vasseur and Cox [13], who included investigations linear shear flow in the presence of a wall. Auton studied the lift force on a sphere due to weak shear flow in an inviscid fluid and developed an expression which is similar to Saffman's, but does not depend on viscosity. Interestingly in Auton's formulation, the lift force is proportional to mass flux while in Saffman it scales with the square root of mass flux [10, 11].

This paper briefly introduces the work performed on drag force, and then describes the progress that has been made towards the analysis of the lift force implementation in M-CFD for single deformed bubbles. A test case was developed based on the original work of Tomiyama et al. [5] and promising results are presented and discussed.

2. PRELIMINARY WORK: DRAG

The viscous drag force on a bubble is caused by the relative motion between the two phases and is expressed as

$$F_D = \frac{1}{2} C_D \rho_c A |u_r| u_r \quad (1)$$

where C_D is the drag coefficient, ρ_c is the density of the continuous phase, A is the projected area ($A = \pi d^2/4$), and u_r is the relative velocity ($u_r = u_c - u_d$ with u_c as the velocity of the continuous phase and u_d as the velocity of the dispersed phase).

Various formulations exist for the drag coefficient, as a function of Reynolds number, and in order to test the performance of these formulations, a unit test case was built in the commercially available STAR-CCM+ software, where the only forces acting on a bubble are buoyancy and drag. In the case, air bubbles and water are injected at the bottom of a vertical channel at 1 m/s. From the inlet, the air bubbles are accelerated due to buoyancy but are pulled back due to drag from the surrounding water. The bubbles

reach their terminal rise velocity when the drag force is balanced by the buoyancy force. Several different drag models are tested: constant coefficient (0.44), Schiller-Naumann, Bozzano-Dente, and Tomiyama. The goal of the study is to reproduce the classic terminal velocity plot (shown below in Figure 1) for various bubble diameters.

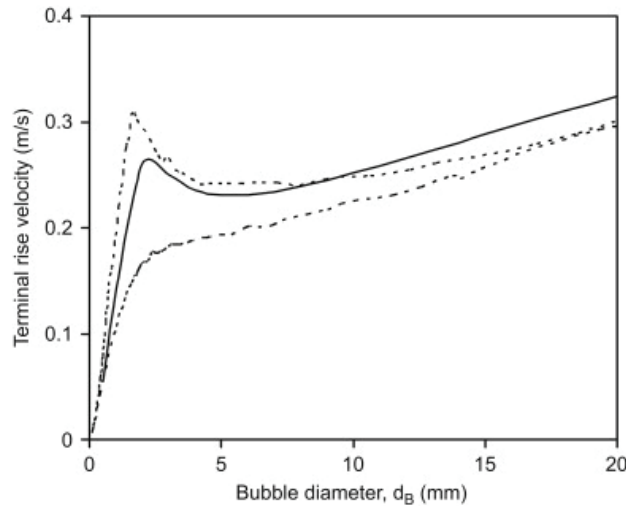


Figure 1. Graph of Terminal Rise Velocity for Various Bubble Diameters.

The balance of forces when the drag force equals the buoyancy force and bubbles reach their terminal velocity is expressed mathematically as:

$$\frac{\pi d^3}{6} \Delta \rho g = \frac{C_D}{2} \rho_c u_r^2 \frac{\pi d^2}{4} \quad (2)$$

The graph in Figure 2 shows the results for terminal rise velocity with respect to bubble diameter for the different drag models.

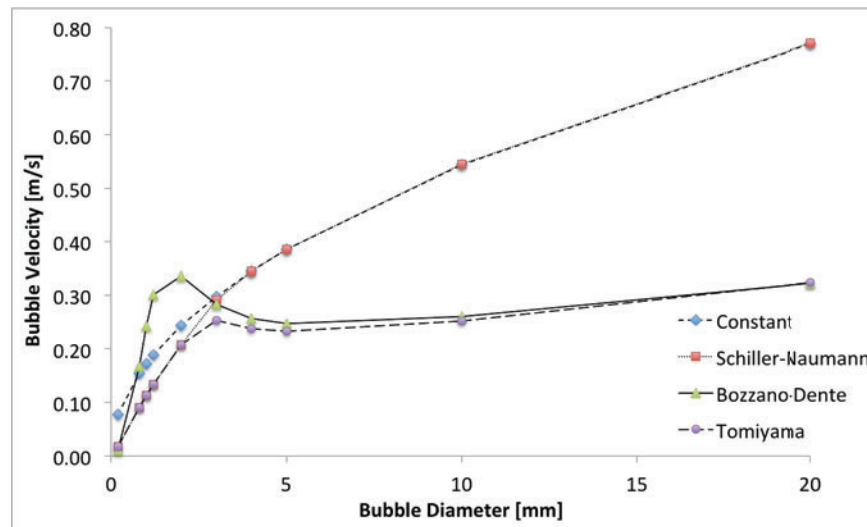


Figure 2. Bubble Terminal Rise Velocity vs. Bubble Diameter for Different Drag Models.

The terminal velocity results show that the drag coefficient correlations which account for non-spherical bubbles (Bozzano-Dente and Tomiyama) all correctly reproduce the expected trend against bubble diameter. Using a constant coefficient or the Schiller-Naumann formulation is a reasonable approximation for small bubbles up to 3 mm, but fails to predict the correct behavior in the higher size range, where the Bozzano-Dente and Tomiyama correlations would be more reliable due to bubble deformation.

3. LIFT FORCE

The lateral lift force on a bubble rising in a liquid is due to the horizontal velocity gradient in the flow. It originates from the inertia effects in the viscous flow around the particle and is expressed as

$$F_L = C_L \alpha_d \rho_c [u_r \times (\nabla \times u_c)] \quad (3)$$

where C_L is the lift coefficient, α_d is the volume fraction of the dispersed phase, ρ_c is the density of the continuous phase, u_r is the relative velocity between the two phases, and u_c is the velocity of the continuous phase. Figure 3 below shows a visual representation of the lift force on a bubble.

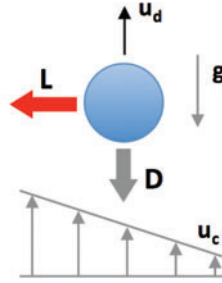


Figure 3. Lift Force on a Bubble.

Numerous formulations exist to describe the lift coefficient, and are specific to a selected flow regime. The most straightforward approach is to assume spherical particles in the lift formulation, which is the basis of the work of Legendre and Magnaudet [6]. On the contrary, a realistic approach requires modeling the influence of bubble deformation, for example in the work of Tomiyama [5] and Hibiki & Ishii [14]. A review of the existing experimental and modeling experience in particular shows that a complete lift formulation should cover three fundamental aspects: lift coefficient variation with bubble diameter, lift force inversion when exceeding a threshold deformation, and near wall behavior, due to bubble wall interaction. In the present work, the last aspect is not discussed and a classic wall lubrication force is adopted. Ongoing work is focusing on the analysis of dedicated experimental and DNS results to extend the lift formulation to the near wall region.

4. LIFT TEST CASES

In order to verify the CFD implementation of the lift force, and further to evaluate the accuracy of existing formulations for the lift coefficient magnitude, a test case was constructed based on the experimental work of Tomiyama [5]. In his work, the transverse lift force is evaluated based on measurements of single air bubble trajectories in simple shear flow of a glycerol-water solution. The simple shear flow with a constant velocity gradient is established with use of a seamless belt, which rotates at a constant speed. Bubbles are injected into the flow through a nozzle with various diameters. The bubble trajectories and shapes are measured, as a function of Morton number M , Eotvos number Eo , and velocity gradient intensity ω , defined below.

$$M = \frac{g(\rho_c - \rho_d)\mu_c^4}{\rho_c^2 \sigma^3} \quad (4)$$

$$Eo = \frac{g(\rho_c - \rho_d)d^2}{\sigma} \quad (5)$$

$$\omega = |\text{rot} \vec{V}_c| = \left| \frac{dV_c}{dy} \right| \quad (6)$$

In the equations above, g denotes the acceleration due to gravity, μ is the viscosity, σ is the surface tension, ρ is the density, V_c is the liquid velocity in the vertical (z) direction, and y is the horizontal coordinate.

4.1. Test Case Setup: Geometry, Mesh, and Physics Conditions

The experimental setup utilized by Tomiyama in his lift study, along with the domain in CFD are presented in Figure 4. The CFD model starts at the bubble injection plane, and extends to just above the measurement plane, where the lateral migrations are measured. The full length of the computational domain is 0.12 m, and the width is 0.03 m with one side representing the moving belt, and the other side representing the far wall. A constant mesh size of 0.5mm is used in the simulations and was selected after a preliminary mesh convergence study.

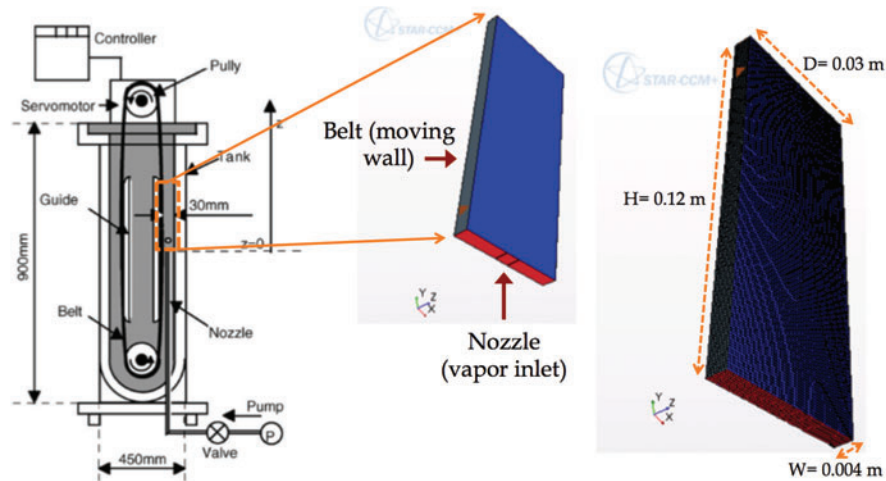


Figure 4. Domain Modeled in CFD from Experimental Setup. Experimental setup image reproduced from Tomiyama [5].

A line probe is set up at 0.1 m downstream from the injection plane, representative of the plane at which experimental data were measured. Void fraction values are collected at this location in the computational simulation, as shown in Figure 5 below.

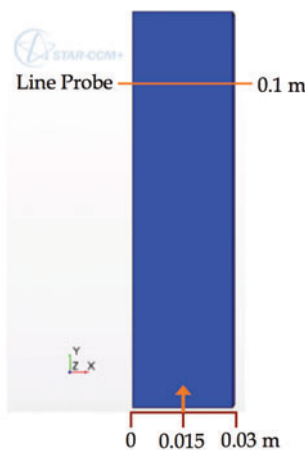


Figure 5. CFD Domain with Injection and Measurement Plane.

As individual bubbles are not resolved in an Eulerian-Eulerian approach, the peak of the void fraction measured at the line probe downstream will represent the migration of a “bubble” from its injection at 15mm. A visual representation is shown in Figure 6. The original peak of the void fraction shows the

bubble at its injection (line probe 4 in yellow). As it travels down the domain, the peak shifts and is captured by line probe 1 in red. The distance between the two peaks represents the bubble's lateral migration due to lift.

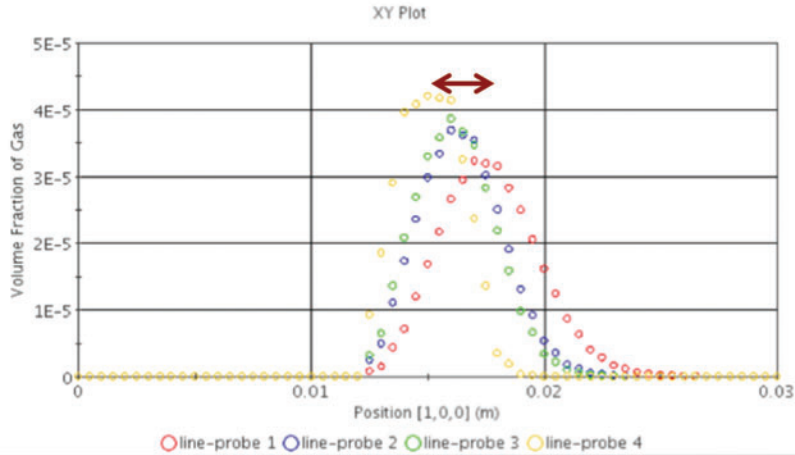


Figure 6. Plot of Void Fraction Peaks at Bubble Injection & Final Measurement Plane.

Another representation of this lateral migration can be seen in the form of a scalar scene, demonstrating the plume of void fraction or “bubble” as it moves down the domain. The bubble's initial position is shown in the left image of Figure 7. Once lift is activated, the plume or bubble shifts and the distance between these two areas of void fraction represents a bubble's lateral migration.

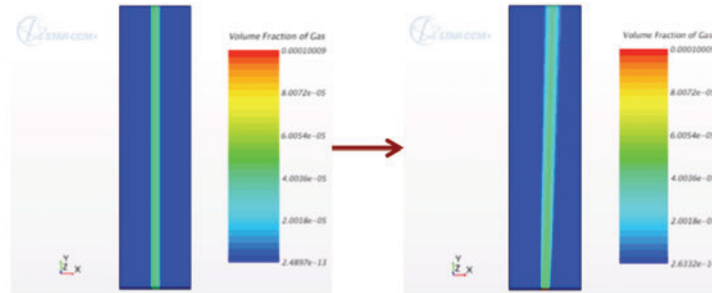


Figure 7. Scalar Scene of Void Fraction with and without Lift Activated.

4.2. Tomiyama's Lift Formulation

Tomiyama's proposed lift formulation based on his experimental data is

$$C_L = \begin{cases} \min[0.288 \tanh(0.121 \text{Re}), f(Eo_d)], & Eo_d < 4 \\ f(Eo_d), & 4 \leq Eo_d \leq 10.7 \end{cases} \quad (7)$$

where:

$$f(Eo_d) = 0.00105 Eo_d^3 - 0.0159 Eo_d^2 - 0.0204 Eo_d + 0.474 \quad (8)$$

$$Eo_d = \frac{g(\rho_c - \rho_d)d_H^2}{\sigma} \quad (9)$$

$$\text{Re} = \frac{\rho_c |V_R| d}{\mu_c} \quad (10)$$

Note that d represents the sphere-volume equivalent bubble diameter, whereas d_H represents the maximum horizontal dimension of a bubble (distortion). See Figure 8 below.

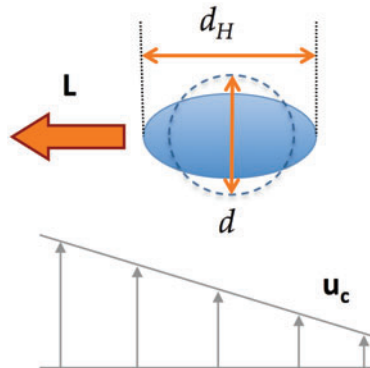


Figure 8. Tomiyama Lift Force Diagram.

The behavior of Tomiyama’s lift coefficient is shown graphically in Figure 9. It can be noticed that small bubbles with a diameter below 0.005 m have a constant positive lift coefficient. Bubbles begin to behave as deformed particles at a diameter larger than 0.005 m, and go from a positive to negative lift coefficient at a diameter of 0.0067 m. A negative lift coefficient corresponds to a negative displacement or lateral migration (to the left in Fig. 8), and a positive lift coefficient corresponds to a positive displacement (to the right in Fig. 8).

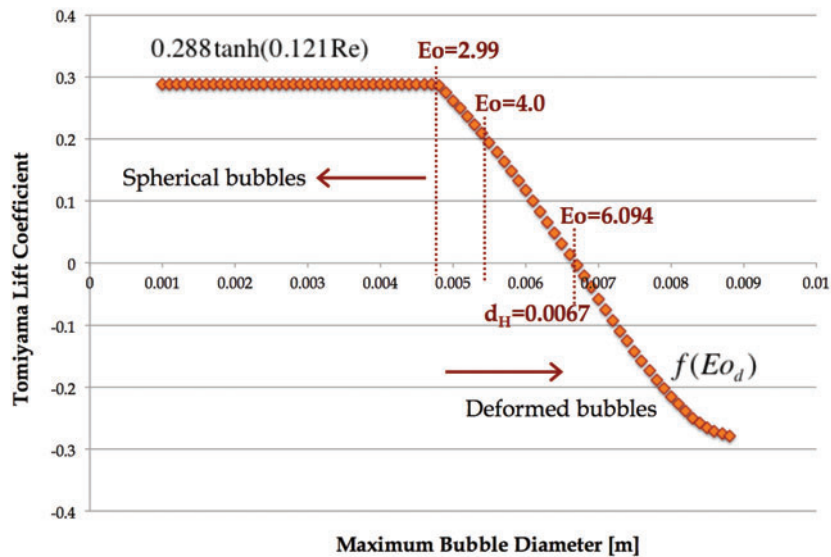


Figure 9. Graph of Tomiyama Lift Coefficient vs. Bubble Diameter.

4.3. CFD Simulations & Results: Failure of Classic Tomiyama Lift in CFD

The first objective of this test case was to study the implementation of the lift force in M-CFD. For this reason, identical implementations were tested in two of the leading commercially available M-CFD solvers, STAR-CCM+ developed by CD-adapco, and ANSYS-CFX developed by ANSYS. Results of this comparison are presented in Figure 10. The remainder of the analyses was performed with the STAR-CCM+ software.

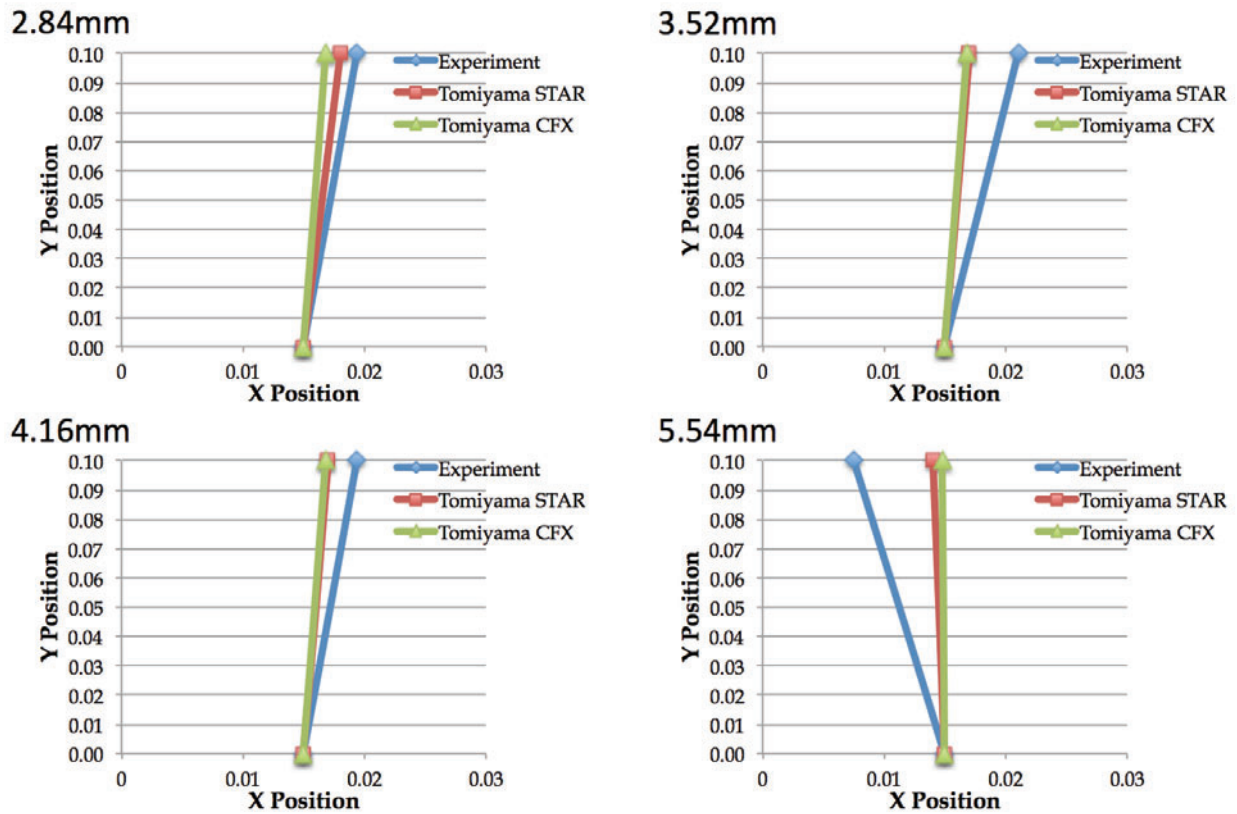


Figure 10. Comparison of Results from STAR-CCM+ and ANSYS-CFX.

The direct comparison of the results from STAR-CCM+ and ANSYS-CFX indicates that the implementation of the lift force is consistent across different M-CFD platforms. Unfortunately, both sets of results are in disagreement with the experimental data from which the lift coefficient correlation was developed. Further analyses have therefore been necessary to shed light on this unexpected finding.

The first series of tests compares numerical results with experimental data for small, spherical bubbles, where constant lift and drag coefficients can be applied. The experimental data used for these tests are shown below in Figure 11.

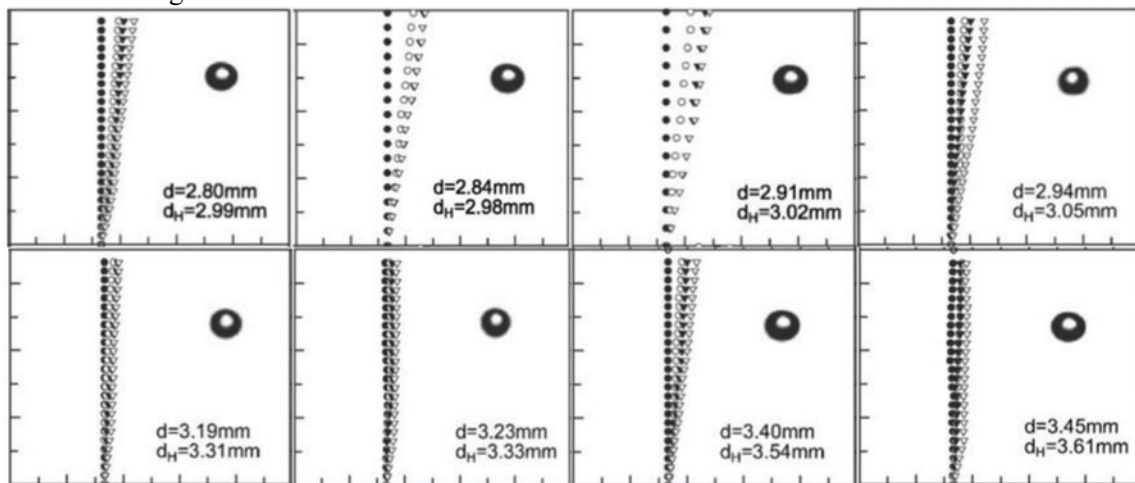


Figure 11. Small, Spherical Bubbles trajectories, reproduced from Tomiyama's Experimental Database [5].

The results from STAR-CCM+, for a constant lift coefficient ($C_L = 0.25$) and drag coefficient ($C_D = 0.44$) are presented in the graphs in Figure 12. The comparison shows a reasonable agreement for the case of small diameter bubbles, with constant lift and drag coefficients.

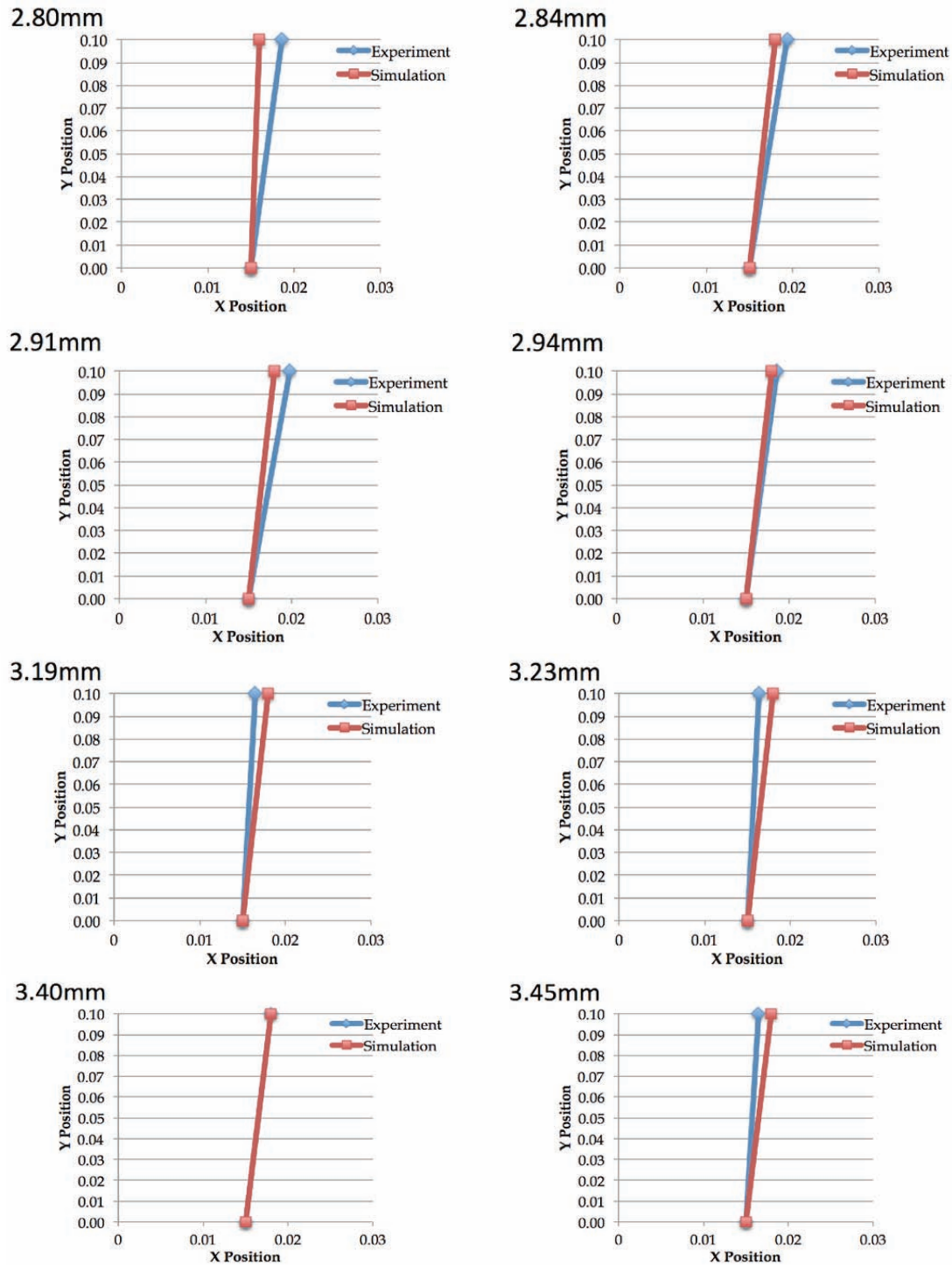


Figure 12. Simulation vs. Experiments for Spherical Bubbles.

Next, four cases were selected to evaluate the prediction for distorted bubbles, and further sensitivity to the lift coefficient magnitude was included in the test. Figure 13 shows the four selected cases, where:

three of the bubbles have positive lift coefficients and positive displacements, while one is so deformed that it has a negative lift coefficient and corresponding negative displacement.

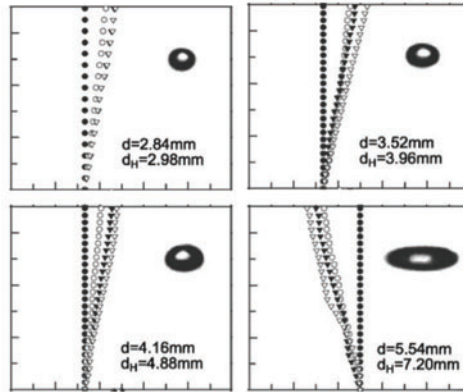


Figure 13. Select Tomiyama Experimental Data for Sensitivity Studies.

Preliminary sensitivity studies were performed on inlet void fraction and solution method (steady-state vs. transient); both sensitivities showed no effect on a bubble's final displacement are not presented here. On the contrary, the sensitivity to the coefficient magnitude is included in the results to appreciate its effect on the predictions.

The results for lift coefficient magnitude on bubble displacement are shown in Figure 14.

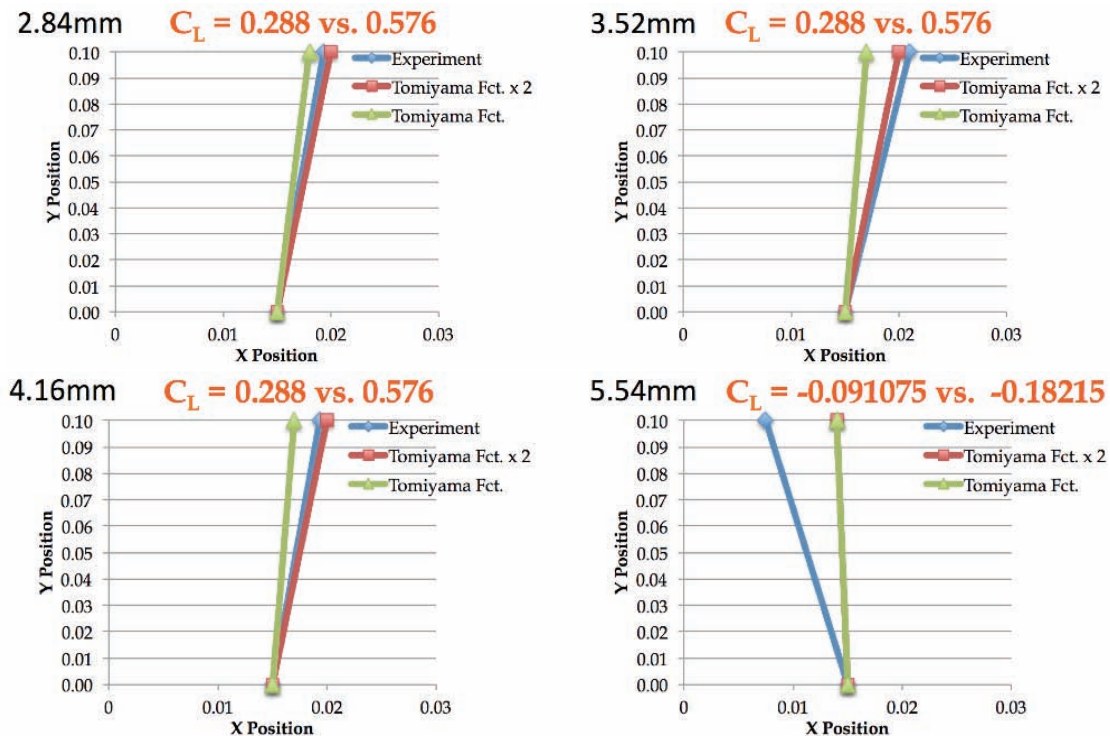


Figure 14. Lift Coefficient Magnitude Sensitivity Results.

It is interesting to notice that for the case of positive lift coefficients (positive displacement), multiplying the coefficient by a factor of two leads to much improved agreement with the experimental results. At the same time, the simulations fail to capture the large negative displacements that result from a negative lift coefficient for larger deformed bubbles, even in the case of higher negative C_L . Further comparisons with

large bubble deformations were therefore performed to analyze this aspect. The large, deformed bubble test cases selected are shown in Figure 15.

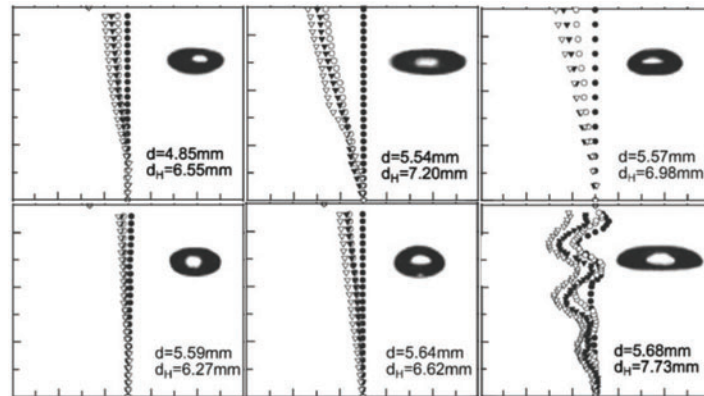


Figure 15. Deformed Bubbles from Tomiyama's Database.

For a purely qualitative analysis, further sensitivities on the coefficient magnitude were performed for the negative lift coefficient cases. Comparisons to the experimental results are shown in Figure 16. The comparisons show that a x10 multiplier to the Tomiyama coefficient would be required to replicate the experimental displacement for larger, significantly deformed bubbles (5.54mm, 5.57mm, and 5.68mm) with negative lift coefficients ($E_o > 6.094$ and $d_H > 6.70$ mm).

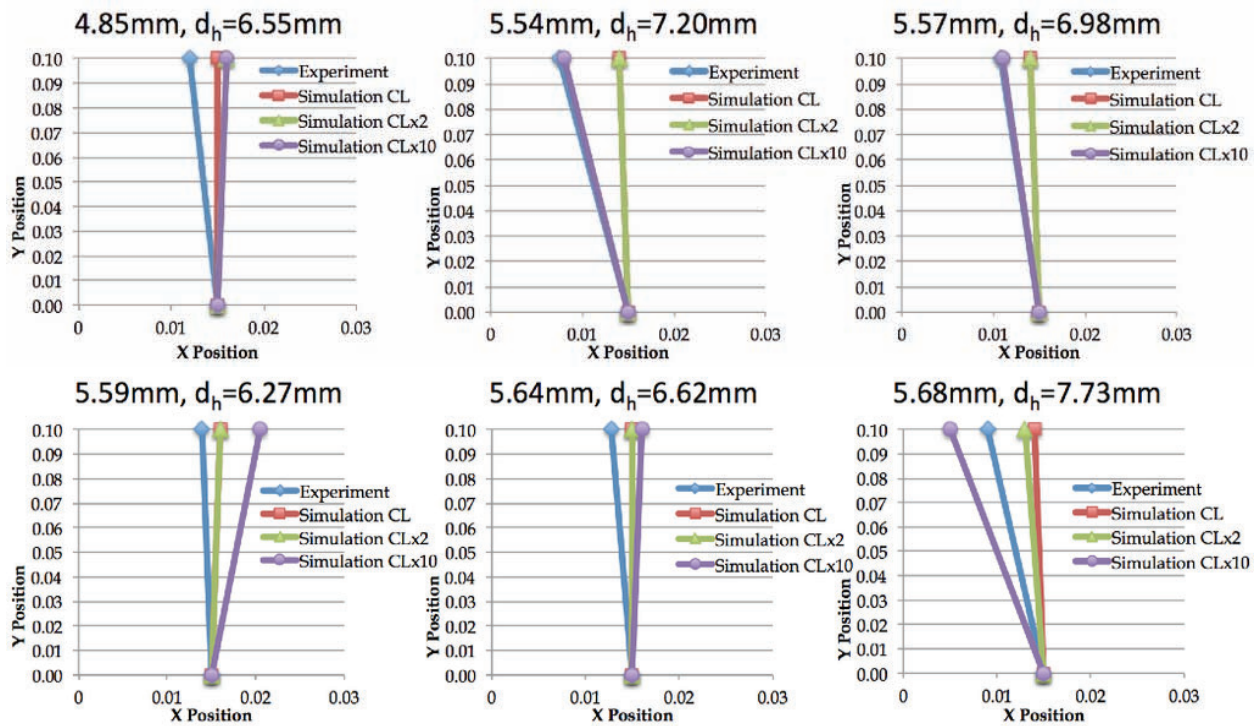


Figure 16. Lift Coefficient Magnitude Sensitivity Study Results for Deformed Bubbles.

In summary, extensive testing and sensitivity analysis of the implementation of the Tomiyama lift coefficient [5] indicate that the closure fails to accurately reproduce experimental bubble displacements when implemented in M-CFD.

5. EXTENSION OF TOMIYAMA WORK & DNS SIMULATION

5.1. Force Balance Analysis

The discussed failure to accurately predict bubble displacements has suggested revisiting the Tomiyama interpretation of the fundamental force balance on a single bubble. The diagram in Figure 17 shows the forces acting on a bubble.

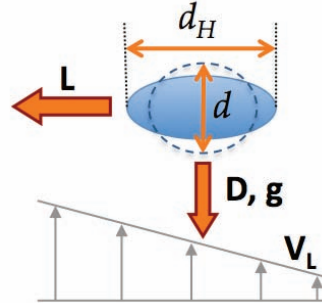


Figure 17. Force Balance on a Bubble.

The equation of bubble motion is given by

$$(\rho_G + 0.5\rho_L)\frac{d\vec{V}_G}{dt} = -\frac{3C_D\rho_L}{4d}|\vec{V}_R|\vec{V}_R - C_T\rho_L\vec{V}_R \times \text{rot}\vec{V}_L + (\rho_L - \rho_G)\vec{g} \quad (11)$$

where V_R is the relative velocity defined as $V_G - V_L$, g is the acceleration due to gravity $(0,0,-g)$, C_D is the Tomiyama drag coefficient, and C_T is the (Tomiyama) lift coefficient. Note that ω is defined as $\text{rot}V_L$.

This expression can be solved for the lift coefficient C_T and the result is:

$$C_T = -\frac{(\rho_G + 0.5\rho_L)}{\rho_L\omega_y\hat{j} \cdot V_R \sin\theta\hat{j}} \frac{2s}{(0.1)^2} [\omega_y s + V_R \cos\theta]^2 \hat{j} \quad (12)$$

where s is the bubble displacement and θ is the angle between the vertical and the direction of the relative velocity. These quantities are shown in Figures 18 and 19.

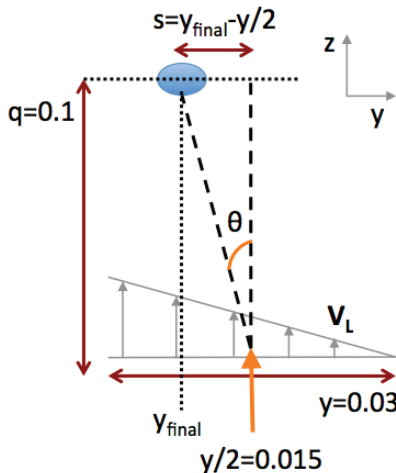


Figure 18. Bubble Schematic for Force Balance Analysis.

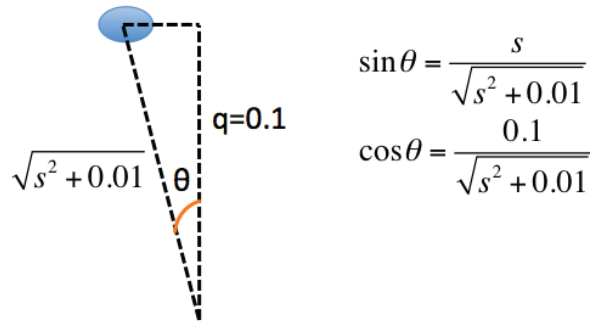
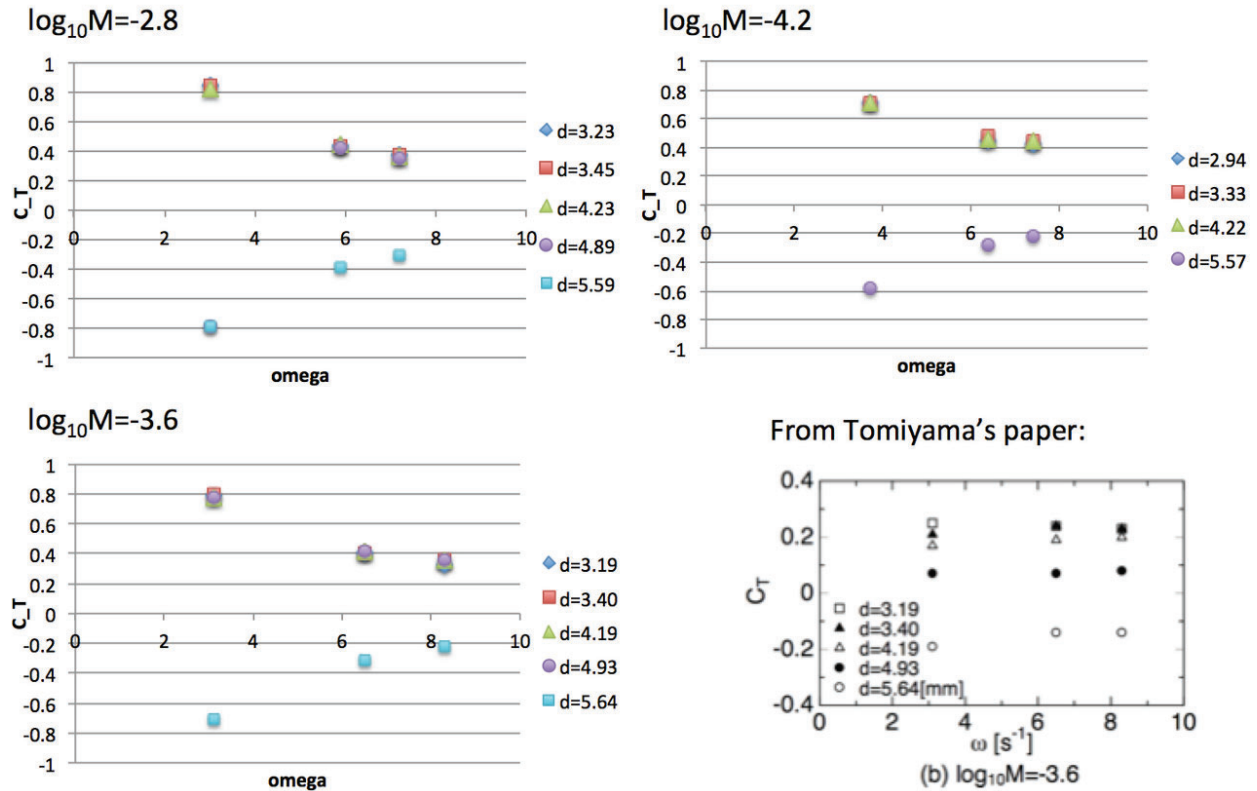


Figure 19. Angle Diagram for Force Balance Analysis.

With this expression in Equation 12, values for the lift coefficient were calculated for the desired experimental conditions and compared with those presented in Tomiyama's 2002 paper [5]. The two sets of data included in Tomiyama's paper are for $\log_{10}M$ of -3.6 and -5.5. These results are shown in Figure 20 below. The two comparisons that can be made, for $\log_{10}M$ of -3.6 and -5.5, indicate that the calculations for lift coefficient are at least double those that were predicted by Tomiyama.



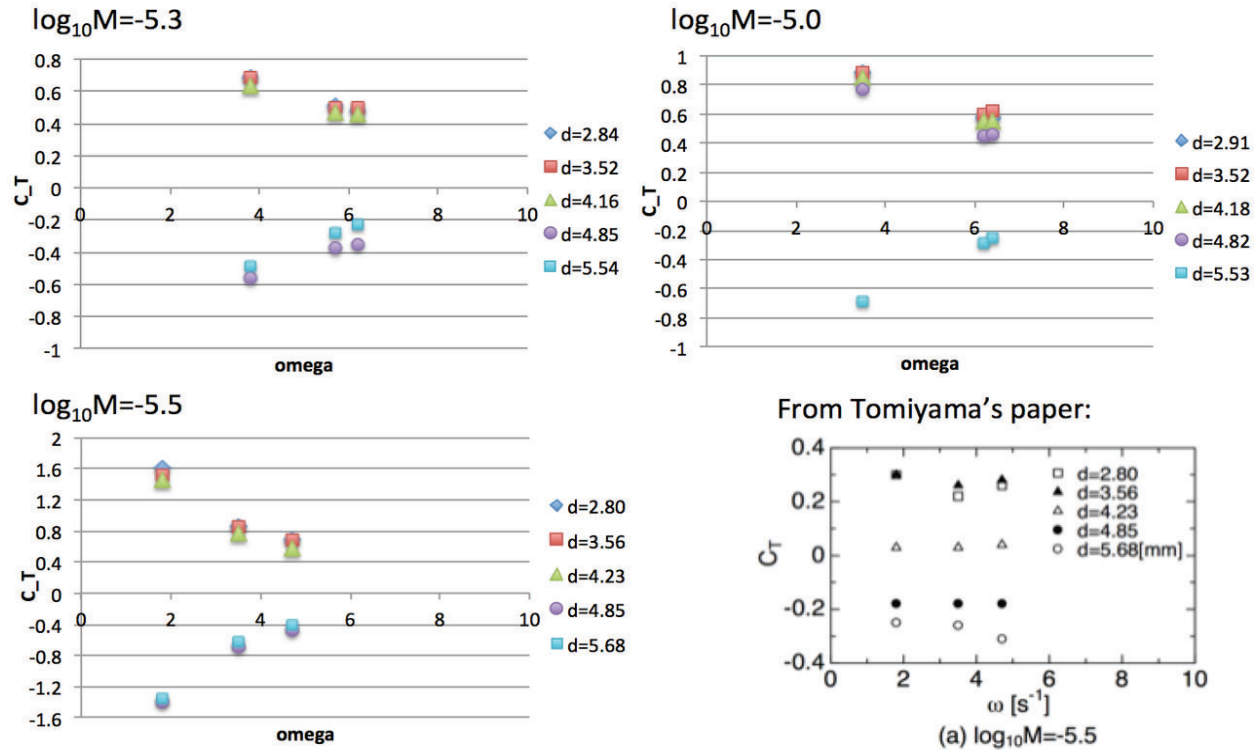


Figure 20. Force Balance Results: Velocity Gradient vs. Lift Coefficient.

5.2. DNS Work

In order to further extend the Tomiyama lift coefficient formulation, in addition to re-evaluating the coefficients as shown in the previous section, the support of DNS simulations is sought, not only to confirm the validity of the approach, but importantly to enlarge the database and therefore applicability of the approach to M-CFD application. The new formulation will be based on Tomiyama's experimental work, along with multiphase DNS data, which will be generated through a collaboration with the group of I. Bolotnov [15], as part of the CASL program [16]. The approach of the DNS simulations is to match the general setup of Tomiyama's experiments and calculate lift force coefficients for various bubble deformations and fluid properties. Bubble deformation is captured by varying the Eotvos and Morton numbers for a set bubble size. The test matrix for the DNS cases that will match CFD simulations and Tomiyama's experiments will include shear rates of 3.8 and 6.2 s^{-1} . One bubble size of 3mm is chosen as a starting point, and surface tension is varied to capture different bubble deformations. Surface tension values are based on the set of Morton numbers used in Tomiyama's experiments, along with the measured bubble sizes. Specifically, the $\log_{10}M$ values used are -2.8, -3.6, -4.2, -5.0, -5.3, and -5.5.

6. CONCLUSIONS & ONGOING WORK

Lift force evaluation in M-CFD has shown that it not only presents a complex implementation challenge, but the state of the art closures adopted in the industry even fail to reproduce the tests they have been developed upon. This work has implemented and tested the Tomiyama lift closure, including extensive sensitivity to modeling and implementation parameters, and has evidenced a fundamental shortcoming in the coefficients formulation.

Validation against Tomiyama's original experiments indicates that the analytical derivation of his lift coefficient formulation does not correctly reproduce the experimental data when implemented in M-CFD.

While the original aim of the project was to extend the lift formulation to group behavior and near wall adaptation, the encountered limitations have driven a refocusing of the objectives.

In order to develop a more general and robust lift closure formulation, a collaborative effort is undergoing as part of the CASL program in which dedicated multiphase DNS results are being generated. These results will be used alongside the experimental data available from Tomiyama's original experiments to formulate a new approach for modeling the lift coefficient, more suitable for CFD applications. Future steps will extend the application and validation of the lift formulation to integral testing, and further extension to higher void fraction regimes.

ACKNOWLEDGMENTS

This work is funded by and would not be possible without the support of the Consortium for Advanced Simulation of Light Water Reactors (CASL). The CFX simulations that were used as a comparison with our results from STAR-CCM+ in our sensitivity analyses for the lift test case were run by Gustavo Montoya Zabala. The DNS work that will be used for the development of a new lift formulation more suitable for CFD is being completed by Igor Boltonov.

REFERENCES

1. W. D. Pointer, A. Tentner, T. Sofu, D. Weber, S. Lo, and A. Splawski, "Eulerian two-phase computational fluid dynamics for boiling water reactor core analysis", *M&C + SNA 2007*, Monterey, California, April 15-19, 2007.
2. F. Takemura, S. Takagi, J. Magnaudet, and Y. Matsumoto, "Drag and lift forces on a bubble rising near a vertical wall in a viscous liquid", *Journal of Fluid Mechanics*, **461**, pp. 277-300 (2002).
3. F. Takemura and J. Magnaudet, "The transverse force on clean and contaminated bubbles rising near a vertical wall at moderate Reynolds number", *J. of Fluid Mech.*, **495**, pp. 235-253 (2003).
4. F. Takemura, J. Magnaudet, and P. Dimitrakopoulos, "Migration and deformation of bubbles rising in a wall-bounded shear flow at finite Reynolds number", *J. of Fluid Mech.*, **634**, pp. 463-486 (2009).
5. A. Tomiyama, H. Tamai, I. Zun, S. Hosokawa, "Transverse migration of single bubbles in simple shear flows", *Chemical Engineering Science*, **57**, pp. 1849-1858 (2002).
6. D. Legendre and J. Magnaudet, "The lift force on a spherical bubble in a viscous linear shear flow", *J. of Fluid Mech.*, **368**, pp. 81-126 (1998).
7. M. Rastello, J.L. Marie, and M. Lance, "Drag and lift forces on clean spherical and ellipsoidal bubbles in a solid-body rotating flow", *J. of Fluid Mech.*, **624**, pp. 434-459 (2011).
8. M. Rastello, J.L. Marie, N. Grosjean, and M. Lance, "Drag and lift forces on interface-contaminated bubbles spinning in a rotating flow", *J. of Fluid Mech.*, **624**, pp. 159-178 (2009).
9. P.G. Saffman, "The lift on a small sphere in a slow shear flow", *J. of Fluid Mech.*, **22**, pp. 385-400 (1965).
10. T.R. Auton, "The lift force on a spherical rotational flow", *J. of Fluid Mech.*, **183**, pp. 199-218 (1987).
11. T.R. Auton, J.C.R. Hunt, and M. Prud'Homme, "The force exerted on a body in inviscid unsteady non-uniform rotational flow", *J. of Fluid Mech.*, **197**, pp. 241-257 (1988).
12. J.B. McLaughlin, "The lift on a small sphere in wall-bounded linear shear flows", *J. of Fluid Mech.*, **246**, pp. 249-249 (1993).
13. P. Vasseur and R.G. Cox, "The lateral migration of spherical particles sedimenting in a stagnant bounded fluid", *J. of Fluid Mech.*, **80**, pp. 561-591 (1977).
14. T. Hibiki and M. Ishii, "Lift force in bubbly flow systems", *Chemical Engineering Science*, **62**, pp. 6457-6474 (2007).
15. I. Boltonov, "Influence of bubbles on the turbulence anisotropy", *J. of Fluids Engineering-Transactions of the ASME*, **135(5)** (2013).
16. "CASL: The Consortium for Advanced Simulation of Light Water Reactors", http://web.ornl.gov/sci/nsed/docs/CASL_Overview.pdf (2013).